



The coupled effect of mechanical and thermal conditions on pedestrian-level ventilation in high-rise urban scenarios

Weiwen Wang^{a,b,*}, Xuemei Wang^{a,b}, Edward Ng^{c,d,e}

^a Institute for Environmental and Climate Research, Jinan University, Guangzhou, 511443, China

^b Guangdong-Hong Kong-Macau Joint Laboratory of Collaborative Innovation for Environmental Quality, Guangzhou, 511443, China

^c School of Architecture, The Chinese University of Hong Kong, Hong Kong, China

^d Institute of Future Cities, The Chinese University of Hong Kong, Hong Kong, China

^e Institute of Environment, Energy and Sustainability, The Chinese University of Hong Kong, Hong Kong, China

ARTICLE INFO

Keywords:

Urban ventilation
High-rise high-density
Mechanical turbulence
Thermal turbulence
Large-eddy simulation

ABSTRACT

Complex urban structure and thermal conditions jointly determine the complexity of urban air flow, but the coupling effect of mechanical and thermal processes on pedestrian-level ventilation has rarely been documented. Using large-eddy simulation (LES) of the idealized wind environment in parametric urban-like geometric scenarios, we evaluated the coupling effect of structural properties and the strength of sensible heat flux of urban blocks on urban ventilation. The study focused mainly on high-rise and high-density urban scenarios, and it was found that for an array of tall buildings, the width of streets perpendicular to the input wind should be considered in defining flow regimes. Canonical flow regimes could be “horizontally” applied to pedestrian-level ventilation because the horizontal wake interference between perpendicular and parallel streets slows down the mean wind in the parallel street canyons. Thermal conditions enhance pedestrian-level ventilation through intensifying vertical mixing by thermal turbulence under weak background wind. However, if the initial thermal conditions are fixed, higher absolute wind speed means stronger horizontal convection, which will weaken the vertical mixing caused by thermal turbulence and eventually lead to the weakening of pedestrian-level ventilation.

1. Introduction

Urbanization is one of the many results of human social development. However, rapid urbanization causes many problems such as urban heat islands and air pollution, which threaten the health of city inhabitants [1–3]. Urban ventilation is one solution to mitigate these problems, as it benefits both thermal comfort in hot weather and pollutant dispersion in street canyons [4–6]. Hence, outdoor ventilation is very important for high-quality and healthy living, particularly in high-rise and high-density cities in tropical and subtropical regions with a hot and humid climate. Nowadays, studies for pedestrian-level wind assessment are receiving plenty of attention due to their rising importance in improving urban living environments in areas of accelerating urban sprawl [7,8].

Complex urban structure leads to complexity of airflow, which arises mainly from turbulence generated by mechanical and thermal processes. Various research methods have been used to describe the complex turbulent flows over urban environments. Computational fluid dynamics

(CFD) techniques, including the Reynolds-averaged Navier-Stokes (RANS) model, large-eddy simulation (LES), and direct numerical simulation, are among the commonly used tools [9–11]. The literature on the CFD of urban ventilation in terms of adopting neutral assumptions, i.e., considering only mechanical process, as well as considering thermal conditions, is briefly reviewed.

1.1. Urban ventilation under neutral conditions

Turbulent airflow in urban areas is strongly influenced by the three-dimensional urban form [12]. As a combination of individual shapes, building dimensions, and their arrangement in the city, urban morphology and urban density can be described by geometric parameters. Parametric studies, which simplify actual urban geometries into idealized scenarios, are widely applied in urban ventilation studies for their advantage of linking specific factors to ventilation performance. Moreover, the CFD tools used in parametric studies are generally more convenient than physical models. Many parameters used to describe the

* Corresponding author. Institute for Environmental and Climate Research, Jinan University, Guangzhou, 511443, China.

E-mail address: wwangeeci@jnu.edu.cn (W. Wang).

<https://doi.org/10.1016/j.buildenv.2021.107586>

Received 21 September 2020; Received in revised form 7 December 2020; Accepted 1 January 2021

Available online 7 January 2021

0360-1323/© 2021 Elsevier Ltd. All rights reserved.

surface cover and structural properties of urban systems are considered in parametric studies of urban ventilation, including urban cover parameters such as building coverage ratio; length scale parameters such as building dimensions, building spacing, and street canyon aspect ratio; and urban structural parameters such as frontal area density [13,14].

Previous studies on air flows in idealized street canyons have indicated that aerodynamic resistance was controlled systematically by both the street canyon aspect ratio and the urban boundary layer (UBL) depth; using a friction factor alone was sufficient to estimate street-level ventilation performance [15]. Lin, Hang [16] investigated urban canopy-layer ventilation with a uniform value of 0.25 in both building coverage ratio and frontal area index, and the effects of urban size, building height, overall urban form, and ambient wind direction were quantified and assessed. Additionally, ventilation in dense building arrays with building coverage ratio values like those of typical European cities was explored, and it was found that the breathability of compact cities could be evaluated using building ventilation concepts (mean flow rate and age of air), as well as vertical mean and turbulent fluxes quantifiable through a bulk exchange velocity [7].

Building height variability enhances vertical mixing and hence influences urban ventilation, but its effects remain incompletely explored. Both wind tunnel tests and CFD simulations have been used to investigate the impacts of building height variation and building density on flow adjustment in idealized urban models [5]. Other parameters include approaching wind direction [16–18], building porosity [19], half open spaces [20], and arcade and lift-up designs [21–24], which may also have an impact on urban ventilation. Following a review of CFD studies of outdoor ventilation for generic urban configurations, Ramponi, Blocken [25] indicated that there was a lack of studies of urban configurations in which all parallel streets do not have equal widths; this initiated their CFD simulation of ventilation in generic urban configurations with different urban densities, and equal and unequal street widths. A parametric study of angular road patterns and pedestrian ventilation in high-density urban areas suggested that the flow field should be affected by both the prevailing wind direction and the relative orientation of adjacent road segments [26].

However, there are still many uncertainties in practical CFD simulations of the pedestrian-level wind environment. For example, following a non-exhaustive literature review of CFD studies on atmospheric processes in street canyons, Ai and Mak [27] indicated that there were arbitrary selections of computational settings in terms of computational domain, domain dimensions, and inflow boundary conditions. In order to improve the quality of simulations of pollutant dispersion in building arrays, Dai, Mak [28] evaluated computational and physical parameters including turbulence models, grid resolution, discretization of time step size, length of sampling period, aspect ratio of arrays, and release rate of tracer gas for CFD simulations. Liu, Pan [29] conducted a CFD study to explore the use of wind information from a meteorological station to simulate wind distribution in an urban community, where the station was located far away from the community. Additionally, Blocken, Stathopoulos [11] reviewed pedestrian-level wind studies for wind comfort assessment using wind tunnel and CFD techniques.

1.2. Effects of thermal conditions on urban wind

As reviewed above, wind tunnel experiments and CFD models have been used in parametric studies of urban ventilation generally with a neutral assumption, which is commonly used mainly because of its low computational cost and the ease with which it can achieve both numerical simulations and wind tunnel experiments. However, thermal conditions are known to have great effects on air flow and turbulence in the urban boundary layer [30,31]. For example, based on an LES study, Nazarian and Kleissl [32] found that heating of roofs, building walls, and the ground was important in the strength and location of a canyon vortex. Within an idealized building array, the thermal effects on turbulent coherent structures were investigated by LES [33], and the results

suggested that when thermal effects of surface heating were included, the spanwise flow was stronger compared with that of the neutral case. Considering different unstable thermal stratification scenarios, Mei, Liu [34] studied pedestrian-level pollutant transport in street canyons. Additionally, on a city scale, Wang and Li [35] used a CFD model to reproduce urban heat island circulation, which has been considered one of the most difficult problems in CFD.

Furthermore, using RANS simulations of two simplified city models, Yang and Li [36] pointed out that airflow in street canyons was dependent on thermal stratification when the wind speed was small relative to the buoyancy force. Taking real building geometries on the Kowloon Peninsula of Hong Kong as a case in a pair of large-domain LES studies, Gronemeier, Raasch [37] indicated that significant ventilation increased in unstable stratification due to enhanced vertical mixing. With daytime observations in Hong Kong, Wang and Ng [38] demonstrated that unstable conditions were more common during summer in the daytime, and hence cross-comparisons of field measurements, wind tunnel tests, and LES under neutral and unstable conditions were conducted. In summary, all the above studies demonstrate the qualitative effect of thermal conditions on urban ventilation in realistic urban complexity.

However, it remains unclear how the above two factors, i.e., urban form and thermal condition, jointly influence pedestrian-level ventilation. The influence of urban form on air flow is mechanical, while urban heat affects air flow around buildings through buoyancy and thermal turbulence. Competition between these two would result in different dynamic stability of the atmosphere. Therefore, it is practical to ask how they affect urban ventilation. The objective of this study is to clarify the coupled effects of urban form and thermal conditions on pedestrian-level ventilation through various sets of parametric scenarios using LES experiments.

2. Scenario configurations

In order to evaluate the effects of urban form and thermal conditions on urban ventilation, urban structures were idealized with a few morphological configurations so that their influences on pedestrian-level ventilation could be investigated and identified. The parametric scenarios were relatively simple in terms of geometric setting but were still based on previous studies. Four design and planning parameters and their combinations were considered: building aspect ratio (which affects mainly the width ratio between perpendicular and parallel streets),

Table 1

Prescribed values and nomenclature of parameters in defining parametric scenarios.

Parameters	Prescribed values	Nomenclature	
Geometric	Mean building height (H)	30 m 60 m	H30 H60
	Building aspect ratio (X)	1:1 2:1	X1 X2
	Building height differential	Homogeneous	HM
		Inhomogeneous	IM
	Building coverage ratio (CR)	25% 40%	CR1 CR2
	Dynamic initialization (input velocity)	1.5 m s ⁻¹ 3.0 m s ⁻¹	V1.5 V3.0
Thermal condition		Neutral Rooftop and side walls heat flux 0.01 Kms ⁻¹ Rooftop and side walls heat flux 0.02 Kms ⁻¹ Rooftop, east and west walls heat flux 0.01 Kms ⁻¹ , south walls heat flux 0.02 Kms ⁻¹ Surface and rooftop heat flux 0.01 Kms ⁻¹	N T1 T2 T3 T4

mean building height, building height differential, and building coverage ratio (Table 1).

First, a floor area including street areas around the building was assumed to be $100\text{ m} \times 100\text{ m}$ (10000 m^2), and the building was in the middle of this floor area. Each parametric scenario was a composite of 10×10 building arrays. Therefore, the site area was 1 km^2 . A three-dimensional schematic diagram of the parametric scenario setup is shown in Fig. 1. The first geometric parameter to be included was the horizontal building aspect ratio; two types of horizontal building aspect ratios were considered. X1 represents a 1:1 ratio of frontal building size (D) to lateral building size (L) (a square), while X2 indicates a ratio of 1:2 (a rectangle). Then, a building coverage ratio (CR) was assumed as 25% or 40%. In this case, the horizontal building-street layouts were computed as follows:

$$D \times L = 100^2 \times CR \quad (1)$$

$$W_s = 100 - D \quad (2)$$

$$W'_s = 100 - L \quad (3)$$

Where W_s and W'_s are the parallel and perpendicular street width, respectively. In the case of X1, $D = L$, and for X2, $L = 2D$.

The next geometric parameters to be investigated were mean building height and building height differential. This study is devoted to providing planning and building advice for tropical and subtropical high-density Asian cities like Hong Kong, where the urban canopy-layer height is about 60 m [10]; thus a mean building height of 60 m (H60) was assumed in most scenarios. But as a supplement, a mean building height of 30 m (H30) was also investigated in some scenarios. In cases of homogeneous building height (HM), all buildings on-site were 60 m (or 30 m); in cases of inhomogeneous building heights (IM), building heights were generated by normally distributed random series, which were given a mean of $H = 60\text{ m}$ (or $H = 30\text{ m}$) and a standard deviation of $H/4$. According to the tolerance intervals of normal distribution, a standard deviation of $H/4$ could basically ensure (99.99%) that no negative random building heights would be generated.

The configurations resulted in eight combinations of urban form except mean building height: X1HMCR1, X1HMCR2, X1IMCR1, X1IMCR2, X2HMCR1, X2HMCR2, X2IMCR1, and X2IMCR2. The building height differential and aspect ratio parameters fixed the building volume (i.e., housing requirement), while the mean building height and building coverage ratio modified the building volume. In cases of H60, the building volume of the four CR1 scenarios was fixed at $1.5 \times 10^5\text{ m}^3$, while the building volume of the four CR2 scenarios was $3.6 \times 10^5\text{ m}^3$. In cases of H30, the building volume was half that of H60.

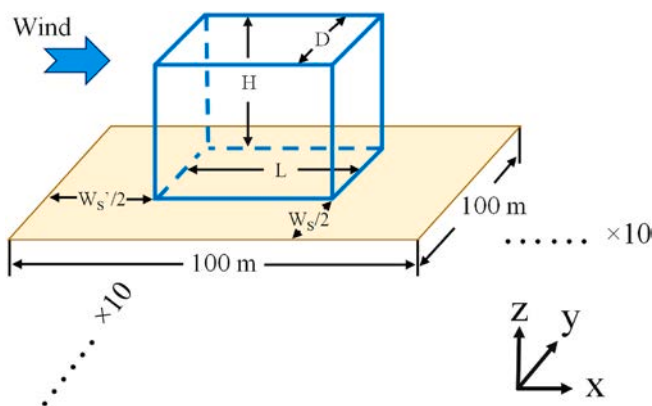


Fig. 1. A three-dimensional schematic diagram of the parametric scenario setup. The floor area, including street areas around the building, is $100\text{ m} \times 100\text{ m}$. The building is in the middle of the floor area. Each scenario is a composite of 10×10 building arrays.

Finally, horizontal dimensions (building sizes and street widths) were computed according to Table 1 and Eqs. (1) – (3). All values were coerced to the closest even-integral numbers, as the horizontal resolution in the LES experiments (refer to the next section) was 2 m. Moreover, besides these geometric settings, we designed two initial input velocities (namely background wind speeds) and three thermal conditions (Table 1), which will be discussed in more detail in the next section.

3. Large-eddy simulation

3.1. Model basics

The LES model used in this study was the Parallelized LES Model (PALM) [39]. The LES model has six prognostic quantities by default: the velocity components u, v, w on a Cartesian grid; potential temperature; specific humidity or a passive scalar; and subgrid-scale turbulent kinetic energy. The governing equations are based on non-hydrostatic, filtered, incompressible Navier-Stokes equations with the Boussinesq approximation and are filtered implicitly using the volume-balance approach of Schumann [40].

The modified version [41,42] of the 1.5-order Deardorff scheme [43] was used for turbulence closure, and the Temperton algorithm [44] for the fast Fourier transform was used to solve the Poisson equation for the perturbation pressure. For the time integration, a third-order Runge-Kutta scheme [45] was employed, and the advection scheme was used for the second-order scheme of Piacsek and Williams [46]. Alternatively, a fifth-order scheme developed by Wicker and Skamarock [47] could also be utilized. Finally, the Monin-Obukhov similarity theory was applied between the surface and the first grid level, and a Prandtl layer was assumed at each surface.

3.2. Grid sensitivity test

In PALM, the Cartesian topography is based on the mask method [48], which allows for explicit resolution of solid obstacles such as buildings. The grid points in the domain are separated into three types: grid points in free fluid without adjacent walls for which standard code is implemented; grid points next to walls that require additional code; and grid points within obstacles that are excluded from computations. Extra code (wall functions) was executed in grid volumes next to walls. Specifically, the LES model employs two 2-D height index arrays, $nzb_w_inner(j, i)$ and $nzb_w_outer(j, i)$ for the vertical component of velocity to separate the domain into different regions based on the vertical index k . Wall-bounded code was executed for grid points next to vertical walls ($nzb_w_inner \leq k < nzb_w_outer$) and horizontal walls ($k = nzb_w_inner = nzb_w_outer$) [39].

A grid sensitivity study of PALM was conducted by Gronemeier, Raasch [37]. In their study, four simulations with grid spacing sizes of 1 m, 2 m, 4 m, and 8 m were compared; neutral conditions were adopted because turbulent structures were generally larger in the thermal case than in the neutral case, while the latter defined the minimum grid size to be used. It was found that a reduction of grid size from 2 m to 1 m only slightly improved the quality of the representation of the wind field in the city. Because a reduction of grid size by a factor of 2 increased the computational load by a factor of 16, a grid size of 2 m was selected for the main simulations in the current study as a tradeoff between accuracy and computational cost.

3.3. Experimental setups

The velocity ratio was employed as an indicator to quantitatively evaluate pedestrian-level ventilation, which was calculated by V_p/V_∞ . Here V_p was the wind velocity at the pedestrian level (2 m above the ground), and V_∞ was the wind velocity at the top of the boundary layer and was not affected by ground roughness. But in this study, wind speed

at the top boundary was affected by thermal conditions; hence the input velocity at the inflow lateral boundary was used as V_∞ . There are many other ventilation indicators such as purging flow rate, visitation frequency, average residence time, local mean age of air, and air exchange efficiency [25], all of which can be calculated using a CFD technique with the emission of pollutant/tracer gas [49]. The PALM model can compute such emission and ventilation indicators with an embedded Lagrangian stochastic particle model [50]. But in the current study, we focus on the effects of both mechanical and thermal conditions on pedestrian-level wind; hence many morphological scenarios were simulated (64 main runs). To save computational time, only 3D wind and turbulence were modelled and output (without calculation of emission and tracer). In order to provide more comprehensive insight into canopy ventilation, we also analyzed the normalized wind profile, streamline, and Richardson number in the canopy. The bulk Richardson number (Ri_b) under thermal conditions is estimated by:

$$Ri_b = gZ_{CT}(\theta_{CT} - \theta_0) / \{ \theta_0(U_{CT})^2 \} \quad (4)$$

where $g = 9.8 \text{ ms}^{-2}$ is the acceleration of gravity, Z_{CT} is the height of the canopy top (estimated at 120 m in this study because the maximum building height is 120 m according to the scenario configuration), θ_0 is the potential temperature at the bottom (the lowest model level), and θ_{CT} and U_{CT} are the potential temperature and wind speed at the canopy top (120 m), respectively.

As we were focusing mainly on the pedestrian-level velocity ratio, the input wind speed was not important under neutral conditions, and if a high wind speed was used, more computational time would be needed because the time steps, which were optimized in the LES model, had to be shorter. Therefore, a wind velocity of 1.5 ms^{-1} was prescribed to save

computational time; that is, $V_\infty = 1.5 \text{ ms}^{-1}$ [51,52]. However, because the mean wind speed could potentially interact with the thermal structure, a higher velocity of 3.0 ms^{-1} was also tested in some scenarios (Table 1). The Reynolds number in the simulation is:

$$Re = V_\infty H / \mu \quad (5)$$

where V_∞ is the inflow bulk velocity, H is the mean building height, and μ is the molecular viscosity. A realistic Reynolds number of $Re = 10^6$ is used since PALM is designed for the urban boundary layer [53].

A no-slip bottom boundary condition and a free-slip top boundary condition were applied to the horizontal velocity components. Only wind directions parallel to the street canyons input from the left were considered in all cases. Cyclic (periodic) horizontal boundary conditions were adopted in the spanwise direction, while non-cyclic boundary conditions were adopted in the streamwise direction. In the case of cyclic lateral boundary conditions, the solution of the pressure solver was achieved by using a direct fast Fourier transform (FFT). The Poisson equation was Fourier transformed in both horizontal directions; the resulting tridiagonal matrix was solved along the z direction and then transformed back [39]. In the case of non-cyclic boundary conditions, PALM generates time-dependent turbulent inflow by a turbulence-recycling method, which was developed by Lund et al. [54], with some modifications by Kataoka and Mizuno [55]. Fig. 2a provides an overview of the recycling method used in PALM. In front of the simulation domain, a recycling area is attached, and the outflow boundary of this recycling area is the recycling plane, from where the turbulence signal $\phi'(y, z, t)$ is recycled:

$$\phi'(y, z, t) = \phi(x_{recycle}, y, z, t) - \phi_y(z, t) \quad (6)$$

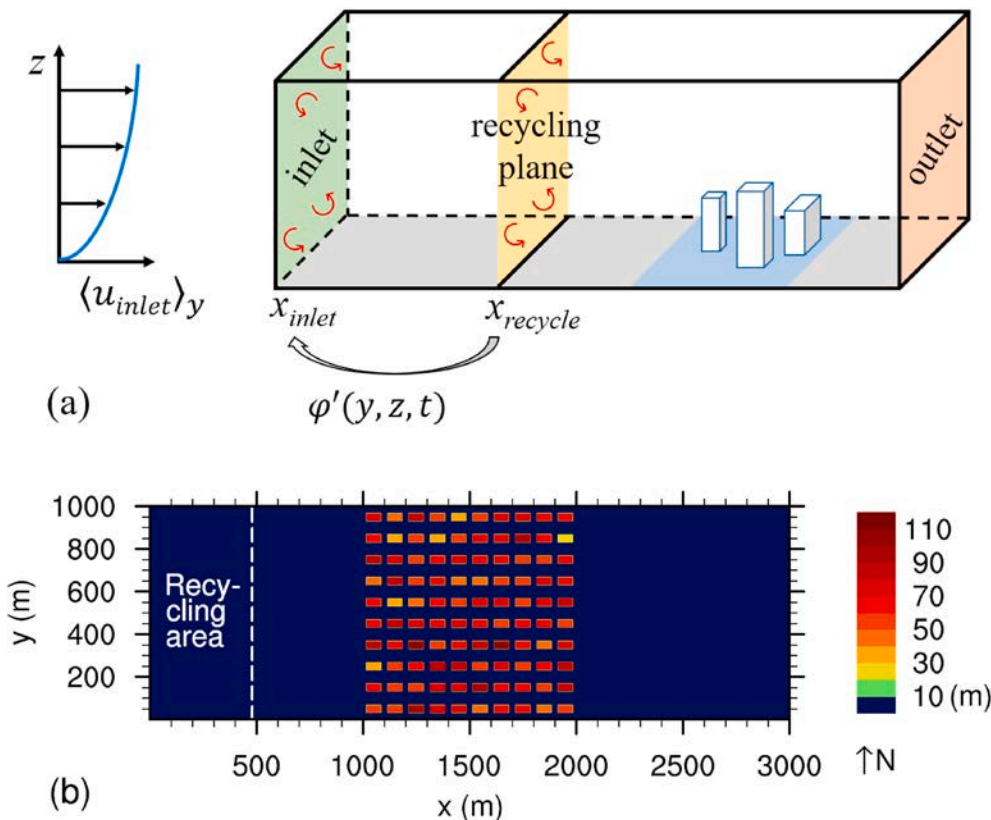


Fig. 2. (a) Schematic figure of the turbulence recycling method modified from Maronga, Gryscha [39]. This configuration represents conditions with an open recycling area (gray surface) and a built-up area for analysis (blue surface). (b) The $3 \text{ km} \times 1 \text{ km}$ LES model domain with the $1 \text{ km} \times 1 \text{ km}$ urban topography (buildings) located in the middle, taking geometric scenario X11MCR1H60 as an example. The white dashed line denotes $x_{recycle}$ (location of the recycling plane) in Eq. (6). (b) demonstrates one of the model setups as an example, which corresponds to geometric scenario X11MCR1H60 (horizontal building aspect ratio 1:1, inhomogeneous building height, building coverage ratio 25%, and mean building height 60 m). The horizontal model domains were $3 \text{ km} \times 1 \text{ km}$, which was adopted from a previous study [38]. In front of the idealized city, a turbulence recycling area was added to the domain, where the turbulence-recycling method was applied to create a turbulent inflow for the simulation. The size of the recycling area was 480 m by 1 km , and it was 520 m away from the city area. The $520 \text{ m} \times 1 \text{ km}$ buffer zone between $x_{recycle}$ and the city helped prevent the blocking effects of the buildings from reaching the recycling area, while the $1 \text{ km} \times 1 \text{ km}$ buffer zone on the leeward side of the city ensured a positive outflow, as the radiative outflow condition in this non-cyclic boundary always required a positive outflow. (For interpretation of the references to color in this figure legend, the reader is referred to the Web version of this article.)

Here x_{recycle} is the distance from the inflow boundary to the recycling plane; $\phi_y(z, t)$ is the line average of a prognostic variable ϕ along y at $x = x_{\text{recycle}}$. $\phi'(y, z)$ is added to the mean inflow profile after each time step. The recycling area length x_{recycle} should be much larger than the integral length scale of the respective turbulent flow to avoid the same turbulence structures being recycled repeatedly. Hence a precursor run, which can have a comparatively small horizontal domain for generating the initial turbulence field of the main run, is promoted [56]. In this case, the domain of the main run was filled by cyclic repetition of the precursor run data. Meanwhile, elements (buildings) were placed sufficiently downstream of x_{recycle} to prevent effects on turbulence at the inlet.

The horizontal grid sizes were equidistantly 2 m, as mentioned above. The vertical grid spacing was 2 m below 300 m and stretched with a stretch factor of 1.08 above. With the 195 vertical levels, the top level was up to 1150 m. The precursor run for the turbulence recycling method has the same grid spacing size and vertical levels as the main run but a much smaller horizontal domain. In this study, the precursor run was set at $240 \text{ m} \times 240 \text{ m}$. The governing equations of PALM were spatially discretized on an Arakawa-C grid. Scalar variables were defined at the grid centers, while the velocity components were shifted by half of the grid spacing. Therefore, the horizontal velocity output from the 1 m and 3 m levels was linearly interpolated to obtain V_p at 2 m above the ground. The total simulation time was 2 h. The first hour was excluded in the analysis, as the turbulence needed this time to spin-up [57], and the simulated results of the last hour were averaged for analysis [58].

For neutral runs, thermal effects were not considered; that is, the temperature equation was shut down. However, for thermal simulations, we considered four sets of heat conditions: (a) a mean kinematic heat flux of 0.01 Kms^{-1} (about 11.75 Wm^{-2}) from both rooftops and side walls, (b) a mean kinematic heat flux of 0.02 Kms^{-1} (about 23.5 Wm^{-2}) from both rooftops and side walls, (c) a mean kinematic heat flux of 0.01 Kms^{-1} from rooftops and east and west walls, and a mean kinematic heat flux of 0.02 Kms^{-1} from the south walls but no heat flux from the north walls, and (d) a mean kinematic heat flux of 0.01 Kms^{-1} from the surface and rooftops but no heat flux from the vertical walls. Four sets of experimental conditions were named T1, T2, T3, and T4, respectively, as listed in Table 1. Among these thermal scenarios, T2 doubled the heating in T1, while T3 and T4 considered two different solar radiation conditions. T3 was comparable to the situation when the sun is at an angle with the land surface; the heat fluxes among walls of different orientations were set to roughly ensure that the total heat flux was consistent with T1. T4 represented the case at noon in the summer, with the sun at its zenith heating only horizontally oriented surfaces [37]. Moreover, unstable stratification in the simulations was achieved by a prescribed homogeneous potential temperature of 300 K below 800 m and a capping inversion layer above with a potential temperature gradient of 1 K per 100 m.

3.4. Model validation

The LES model has been verified for simulating air flows and turbulence characteristics at the street-canyon and neighborhood scale in urban areas [59–62], and the PALM version used in this study has recently been validated by a CFD guideline [63] for pedestrian-level ventilation under neutral atmospheric conditions [64,65]. Regarding the simulation of the thermally stratified urban boundary layer, the model has been tested by Uehara's wind tunnel data [66] for thermally stratified street canyons [67]. In this study, simulations under the neutral assumption were validated by wind tunnel tests, and simulations in thermal conditions were also verified by field measurements. As mentioned above, the model domain setups used in the current study were adopted from a previous study [38], but it is worth noting that the thermal setup was different from that in the literature. The heat fluxes of

both rooftops and side walls were 0.01 Kms^{-1} in the current study (see T1 in Table 1), while in the literature the heat fluxes of side walls and rooftops were 0.01 Kms^{-1} and 0.1 Kms^{-1} , respectively. It should be noted that even with the lower rooftop heat flux (i.e., 0.01 Kms^{-1}), its impact on pedestrian-level ventilation is small, as Fig. 3 demonstrates that the modified heat fluxes (both side wall and rooftop heat fluxes are 0.01 Kms^{-1}) can still capture the observed velocity ratios well.

4. Results

A total of 64 scenario simulations were carried out, as listed in Table 2. There were 8 combinations of urban form except mean building height, and 6 groups in terms of various thermal conditions, mean building heights, and input velocities.

4.1. Mechanical effect of urban form on ventilation

Using the LES results of the parametric urban form scenarios, we first examined the mechanical effect of urban morphology on urban ventilation without considering the thermal effects. Fig. 4 shows LES-computed velocity ratios in the urban area of neutral scenarios with a mean building height of 60 m (H60) and an input velocity of 1.5 ms^{-1} (V1.5), which could indicate detailed influences of urban morphology on pedestrian-level ventilation. When ambient wind encounters the first row of obstacles (buildings), flow separation occurs, indicating that flow near the buildings is highly dynamic. Additionally, flow acceleration occurs in the displacement zone around the buildings and results in very high pedestrian-level velocity on both sides of the first row of buildings. To focus on the urban effects inside the urban scenarios, ventilation around the first row of buildings should be excluded by defining an assessment. It should be noted that all pedestrian-level ventilation statistics were calculated and analyzed inside the assessment area, which reserved a 100 m buffer zone away from the lateral urban edge in all directions (dashed boxes in Fig. 4), and the site-averaged velocity ratios of all 64 tested scenarios are listed in Table 2. The site-averaged velocity ratio is the mean of velocity ratios at $z = 2 \text{ m}$ in the assessment area.

4.1.1. Impacts of building spacing and flow regimes

The site-averaged velocity ratios range from 0.11 to 0.25 for different geometric scenarios under neutral conditions with 60 m mean building height and 1.5 ms^{-1} input velocity (G1 of Table 2). This suggests that pedestrian-level ventilation in scenarios with a building aspect ratio of 2:1 (X2) will be always better than those of X1 scenarios, mainly because X2 scenarios provide wider street canyons parallel to the input wind direction. This indicates that trunk road orientations should keep pace with the summer prevailing wind direction in tropical and subtropical cities that require better summer ventilation. However, Fig. 4 implies that the width of the street parallel to the input wind direction is not the only factor controlling site-averaged ventilation; for example, based on the scenario configurations (Section 2), the parallel street width of the X2CR2 scenarios (54 m) is only slightly greater than that of the X1CR1 scenarios (50 m), but the site-averaged velocity ratios of X2HMCR2 (0.25) and X2IMCR2 (0.21) are much larger than those of X1HMCR1 (0.15) and X1IMCR1 (0.17).

In order to interpret the dynamic contributing factors, simulated flow fields (streamlines) are employed (Fig. 5). Classical urban aerodynamic studies have proposed that building spacing with reasonably uniform building height, i.e. the building height to street width ratio (H/W), could set three canonical flow regimes, which are an isolated roughness flow of $H/W < 0.35$ for widely spaced buildings, $0.35 < H/W < 0.65$ for a wake interference flow at greater densities, and $H/W > 0.65$ for a skimming flow with even closer spacing [13]. Fig. 5 suggests that for an array of very tall buildings, the H/W ratio could be an insufficient indicator of flow regimes. Because we focused on high-rise and high-density urban scenarios (representing the current situation of some Asian cities), the mean building height was set to 60 m. It should be

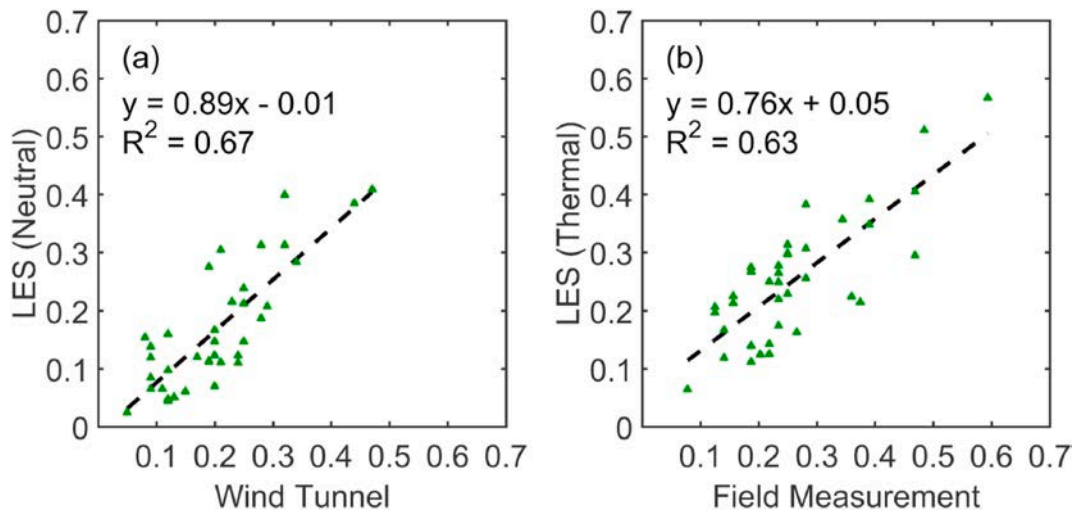


Fig. 3. Velocity ratio scatterplots and regression of (a) wind tunnel and neutral LES and (b) field measurements and diabatic LES. Figures modified from Wang and Ng [38].

Table 2

Parametric combinations of the 64 scenarios and site-averaged velocity ratios in the assessment area. The group ID is given in the last row in order to facilitate interpretation.

Thermal condition		N			T1		T2	T3	T4
Mean building height		H60	H30	H60	H60	H60	H60	H60	H60
Input velocity		V1.5	V1.5	V3	V1.5	V3	V1.5	V1.5	V1.5
Urban form except mean building height	X1HMCR1	0.15	0.20	0.15	0.35	0.20	0.42	0.34	0.35
	X1HMCR2	0.11	0.17	0.12	0.32	0.23	0.40	0.34	0.35
	X1IMCR1	0.17	0.20	0.17	0.32	0.19	0.39	0.31	0.39
	X1IMCR2	0.14	0.17	0.15	0.28	0.18	0.35	0.27	0.34
	X2HMCR1	0.24	0.24	0.26	0.43	0.30	0.48	0.41	0.53
	X2HMCR2	0.25	0.27	0.26	0.44	0.31	0.49	0.42	0.58
	X2IMCR1	0.19	0.23	0.20	0.40	0.23	0.48	0.39	0.44
	X2IMCR2	0.21	0.22	0.21	0.43	0.25	0.49	0.39	0.51
Group ID		G1	G2	G3	G4	G5	G6	G7	G8

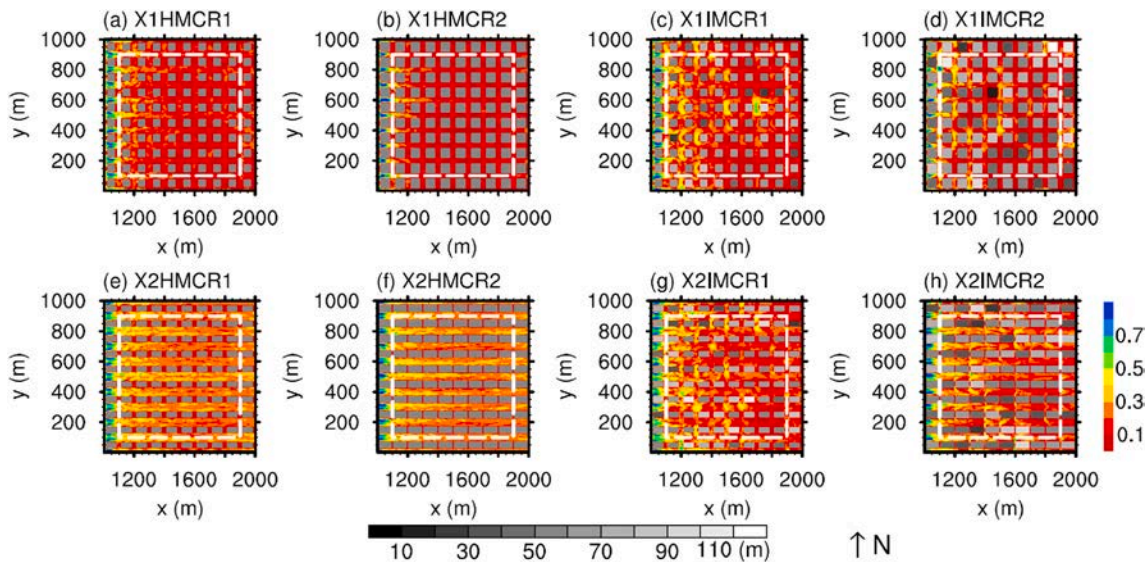


Fig. 4. LES-computed velocity ratio in the urban area of neutral scenarios. Scenarios in G1 (mean building height = 60 m, input wind speed = 1.5 ms⁻¹, neutral conditions) are demonstrated. The dashed white box encloses the assessment area with a 100 m wide buffer zone from the lateral boundary.

noted that this building height is higher than heights commonly used in previous studies [7]. Thus, absolute building spacing or the width of the street perpendicular to the input wind would be important. In this study,

we set the H/W ratios of 1.2, 1.7, 2.0, and 6.0 (Fig. 5a–d, corresponding to the Ws at 50 m, 36 m, 30 m, and 10 m, respectively), which were significantly larger than 0.65. Interestingly, only scenario X2HMCR2

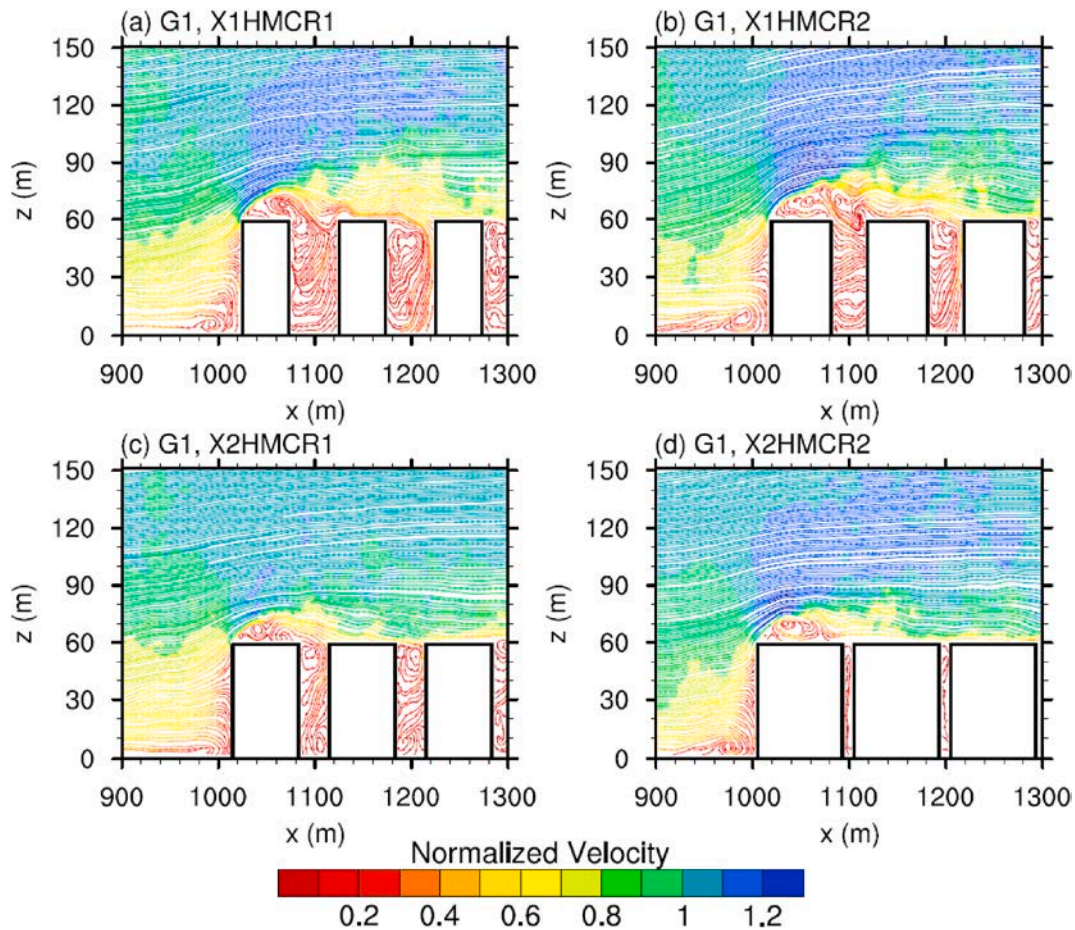


Fig. 5. Vertical streamlines of scenarios (a) X1HMCR1, (b) X1HMCR2, (c) X2HMCR1, and (d) X2HMCR2 in G1 (mean building height = 60 m, input wind speed = 1.5 ms^{-1} , neutral conditions). Color shading is velocity $(u^2+w^2)^{1/2}$ normalized by the input velocity (1.5 m s^{-1}). The section is taken at $y = 550 \text{ m}$. (For interpretation of the references to color in this figure legend, the reader is referred to the Web version of this article.)

(Fig. 5d) demonstrated a skimming flow pattern, while the other three had a wake interference flow.

Fig. 6 demonstrates the streamlines of four G1 scenarios with homogeneous building height (HM). It is found that the canonical flow regimes can be “horizontally” applied to pedestrian-level ventilation. Although the widths of the streets parallel to the input wind are similar, the latitudinal building spacing in Fig. 6a is significantly greater than that in Fig. 6b and results in wake interference flow from the rooftops, and more interestingly, from the lateral ventilating street canyon. The horizontal wake interference between the perpendicular and parallel streets slows down the mean wind in the parallel street canyons. This dynamic process results in G1 scenarios in which, in the case of X1, CR1 (CR = 25%) is better than CR2 (CR = 40%), but in the case of X2, CR2 is close to or even slightly better than CR1 (Table 2 and Fig. 4). But obviously, the narrow perpendicular street widths could lead to a small peak with a low velocity ratio in the distribution, particularly for homogeneous building height (HM) scenarios (Fig. 7).

4.1.2. Balance between mean wind and turbulence intensity

Another statistical feature is that in the case of X1, IM is better than HM, but in the case of X2, HM is better than IM (G1 in Table 2). The downward-propagated momentum flux in IM scenarios is generally stronger than that in HM scenarios, and the stronger vertical momentum flux introduces more wind load to the pedestrian level in high-roughness scenarios that formerly had worse ventilation (X1 scenarios here). Stronger vertical momentum and mechanical turbulence decrease pedestrian-level ventilation in low-roughness scenarios that formerly had better ventilation (X2 scenarios here). In other words,

inhomogeneous building heights generate more vertical momentum in street canyons by capturing more downward-propagated momentum fluxes, and they have a negative (positive) effect on the pedestrian-level velocity of low-roughness (high-roughness) idealized urban fabrics [64], which is supported by previous wind tunnel studies of scalar (e.g., air mass) transfer efficiency [68]. Generally, we suggest that the balance between mean flow and turbulence intensity would be important for ventilating street canyons.

4.1.3. Impacts of canopy height and input wind speed

It is well known that the lower the mean building height, the better the canopy ventilation. Based on the site-averaged velocity ratios of the G1 and G2 scenarios (Table 2), we quantitatively estimated the effect of mean building height, i.e., the height of the urban canopy layer, on ventilation. The rising percentage of the velocity ratio was calculated by subtracting the site-averaged velocity ratio of the H60 scenarios (VR_{H60}) from the site-averaged velocity ratio of the H30 scenarios (VR_{H30}) and then dividing by VR_{H60} as in the following equation:

$$(VR_{H30} - VR_{H60}) / VR_{H60} \times 100\% \quad (7)$$

When urban canopy height decreases from 60 m to 30 m, the increase in the site-averaged velocity ratio ranges from 0% (X2HMCR1) to 54.5% (X1HMCR2), with an average of 20.1% for the eight scenarios, in which the average for the X1 scenarios is 31.0%, and for the X2 scenarios 11.3%. The site-averaged velocity ratios of the X1 scenarios approach those of the X2 scenarios after reducing the average building height. Fig. 7 demonstrates the differences in the velocity ratio distributions in the H30 and H60 scenarios (corresponding to the green and red lines,

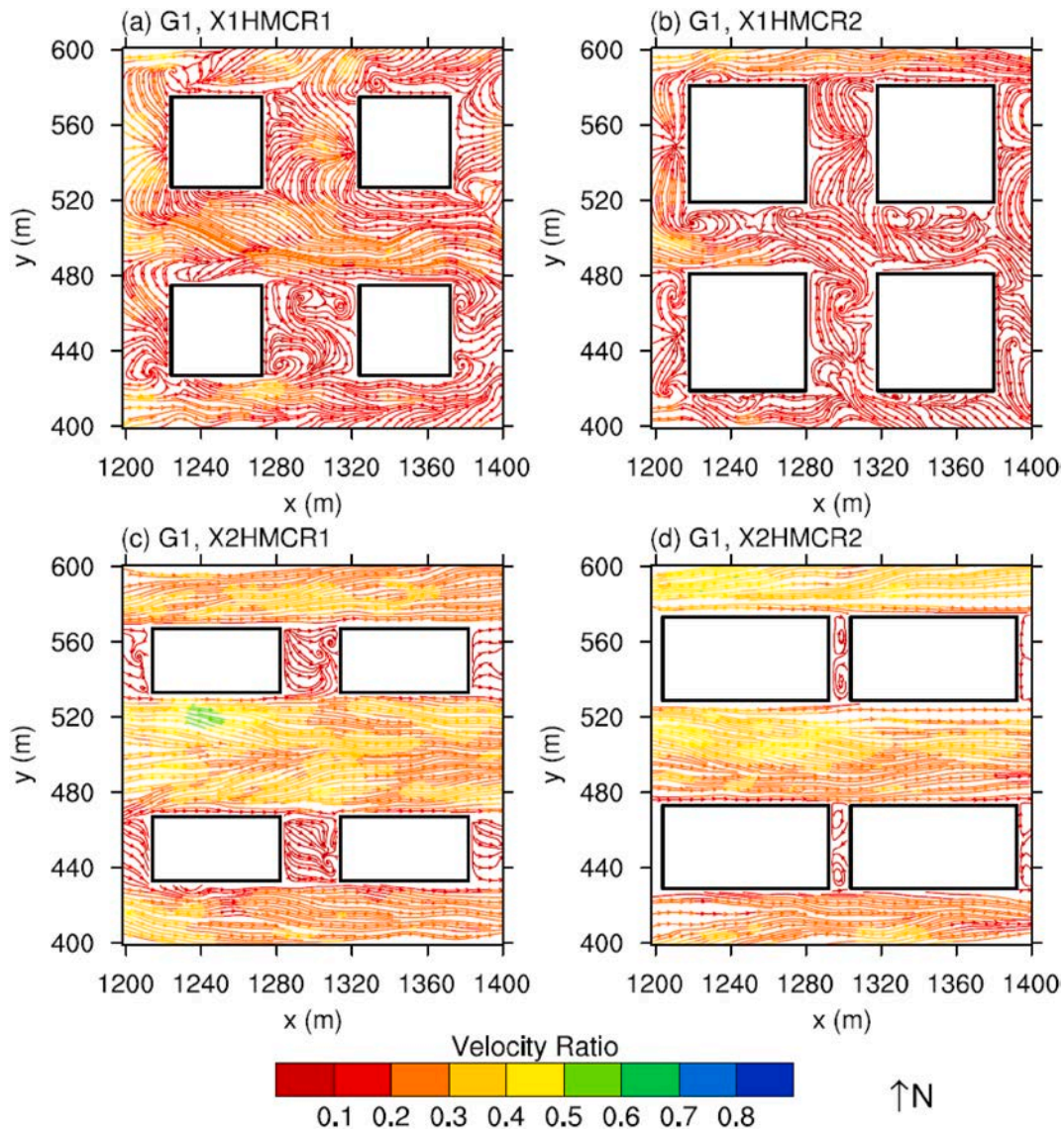


Fig. 6. Horizontal streamlines at 2 m above the ground of scenarios (a) X1HMCR1, (b) X1HMCR2, (c) X2HMCR1, and (d) X2HMCR2 in G1 (mean building height = 60 m, input wind speed = 1.5 m s^{-1} , neutral conditions). Color shading represents the velocity ratio. Only four buildings and the surrounding flow fields are shown. (For interpretation of the references to color in this figure legend, the reader is referred to the Web version of this article.)

respectively), and Fig. 8 illustrates these ventilation differences dynamically by showing the mean wind profiles. The profiles are averaged from 5 y-z sections at $x = 1400 \text{ m}$, 1450 m , 1500 m , 1550 m , and 1600 m . With a lower mean building height, the momentum of mean wind propagation will be deeper into the street canyon (Fig. 8), while the peak of the velocity ratio distribution will shift to the right (with greater velocity ratio) (Fig. 7).

Additionally, a comparison of site-averaged velocity ratios in G1 and G3 suggests that the input velocity should have almost no impact on the simulated pedestrian-level ventilation (Table 2). This demonstrates that it was reasonable to use velocity ratio to describe pedestrian-level ventilation under neutral conditions in previous studies [51,52]. However, this is applicable only in neutral atmospheric conditions; under thermal conditions (in next sections), background wind speed will have a great impact on velocity ratios.

4.2. Impact of thermal conditions on urban ventilation

A comparison of site-averaged velocity ratios in the G1 and G4 scenarios supports the contention that under low background wind speed,

pedestrian-level ventilation in thermal conditions is better than that in neutral conditions (Table 2). Fig. 10 demonstrates the spatial distribution of velocity ratios in urban areas under T1 thermal conditions (G4 scenarios). Compared with the G1 scenarios (Fig. 4), the pedestrian-level ventilation under diabatic conditions is evidently better than that of the neutral conditions.

Enhanced vertical mixing due to surface heating produces improved ventilation performance in the thermal cases [37]. Near-surface velocity over boundary-layer velocity (i.e., velocity ratio) is known to be larger in an unstable atmospheric boundary layer than in a neutral one. Comparing the u-wind profiles of G4 and G6 in Fig. 9 with that of G1 in Fig. 8, it is obvious that the thermal cases produce a greater near-surface velocity than the neutral cases. The higher wind speed in the thermal cases is due to the additional convective motion caused by heating from the buildings, which increases vertical mixing throughout the boundary layer in and above the urban area and leads to the higher pedestrian-level velocity ratios compared to the neutral cases. Furthermore, when other conditions remain unchanged, stronger heating (e.g., T2 compared with T1) results in stronger vertical mixing in and over the urban blocks and hence produces higher velocity ratios.

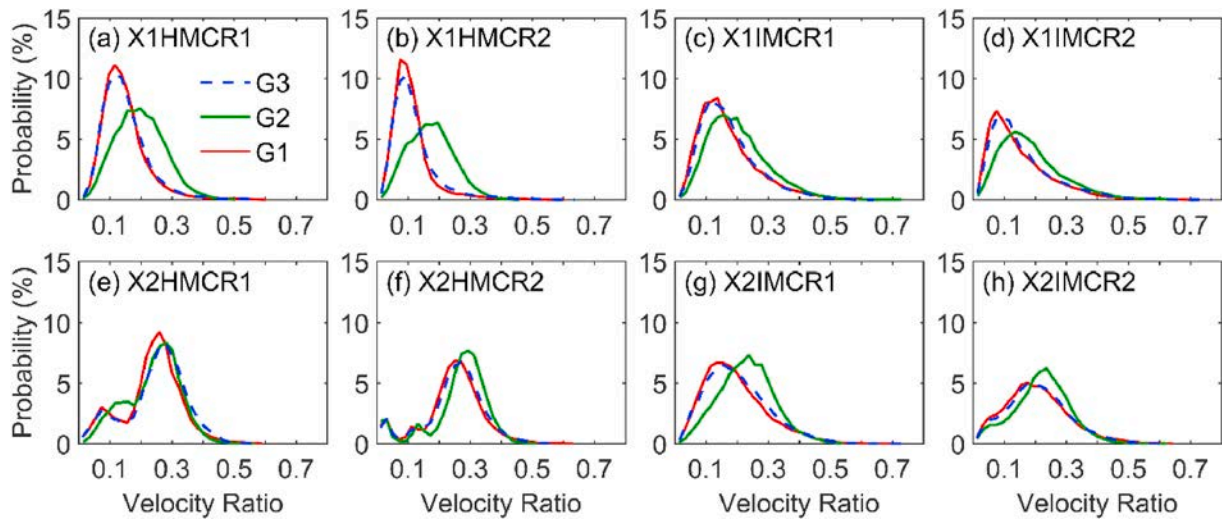


Fig. 7. Pedestrian-level ventilation performance of all neutral scenarios presented by the probability distribution of LES-computed velocity ratios. Each panel presents one urban form combination, and the different line styles (colors) denote different groups (G1, G2, and G3). G1 represents 60 m mean building height (H60) and 1.5 ms^{-1} input velocity (V1.5), G2 represents 30 m mean building height (H30) and 1.5 ms^{-1} input wind speed (V1.5), and G3 represents 60 m mean building height (H60) and 3.0 ms^{-1} input wind speed (V3.0). (For interpretation of the references to color in this figure legend, the reader is referred to the Web version of this article.)

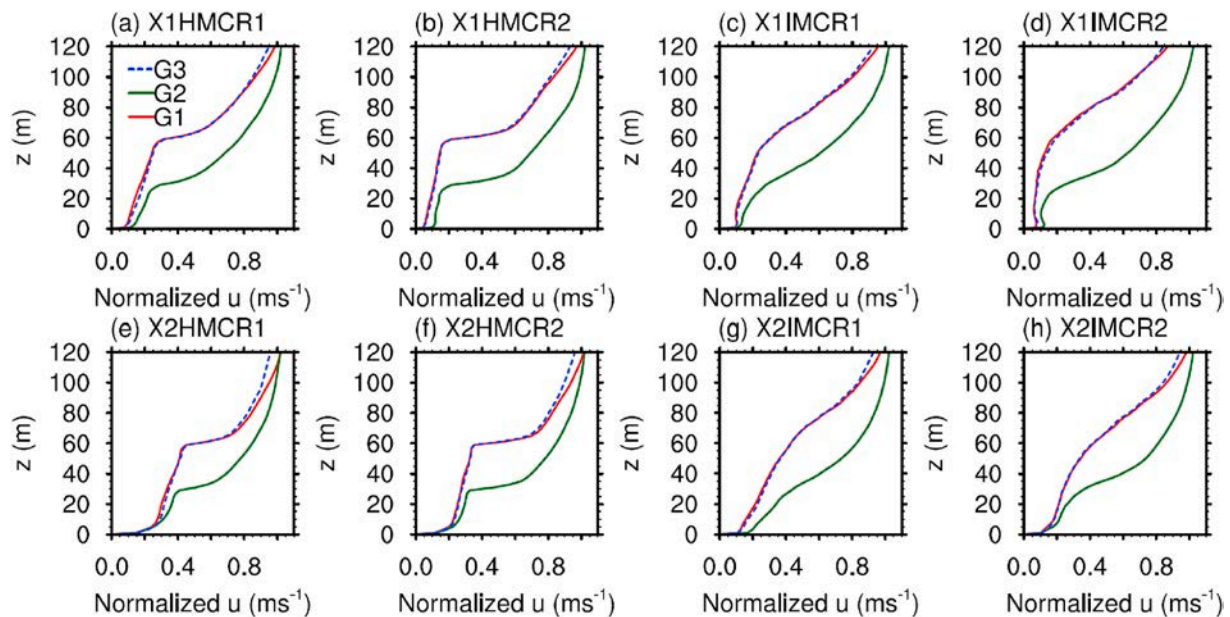


Fig. 8. U-wind profiles in the urban area of neutral scenarios. Only profiles below 120 m are displayed to enlarge the differences between the different scenarios. The profile is normalized by its input velocity. Each panel presents one urban form combination, and different line styles (colors) denote different groups (G1, G2, and G3). G1 represents 60 m mean building height (H60) and 1.5 ms^{-1} input velocity (V1.5), G2 represents 30 m mean building height (H30) and 1.5 ms^{-1} input velocity (V1.5), and G3 represents 60 m mean building height (H60) and 3.0 ms^{-1} input velocity (V3.0). (For interpretation of the references to color in this figure legend, the reader is referred to the Web version of this article.)

As mentioned above, thermal condition T3 prescribes 0.01 Kms^{-1} heat flux from the rooftops and east and west walls, and 0.02 Kms^{-1} heat flux from the south walls, but no heat flux from the north walls. Such differential treatment of the heat flux of the different walls is more realistic than the idealized setting in T1. However, the total heat flux of T3 and T1 is the same, which results in the site-averaged velocity ratios in G7 and G4 being comparable (Table 2). The u-wind profiles in the two groups are similar as well (figure not shown). In general, if the overall heat flux is unchanged, the different heating from vertical walls has little effect on pedestrian-level ventilation.

However, heat flux from the ground surface does improve

pedestrian-level ventilation and increases the overall velocity ratio compared with the heat flux from vertical walls. According to the scenario configuration, T1 scenarios have more heated surface/wall area than T4 scenarios in the case of H60. But the site-averaged velocity ratios in G8 are mostly larger than those of G4 (Table 2). The R_{ib} of 40 scenarios under thermal conditions is estimated and listed in Table 3. Generally, significant linkage between the site-averaged velocity ratio and R_{ib} cannot be found. But the R_{ib} of the T4 scenarios (ranging from -0.43 to -0.28) with ground surface heating is obviously different from that of other scenarios (ranging from -0.15 to -0.1) without a prescribed surface heat flux, mainly because ground surface heating results

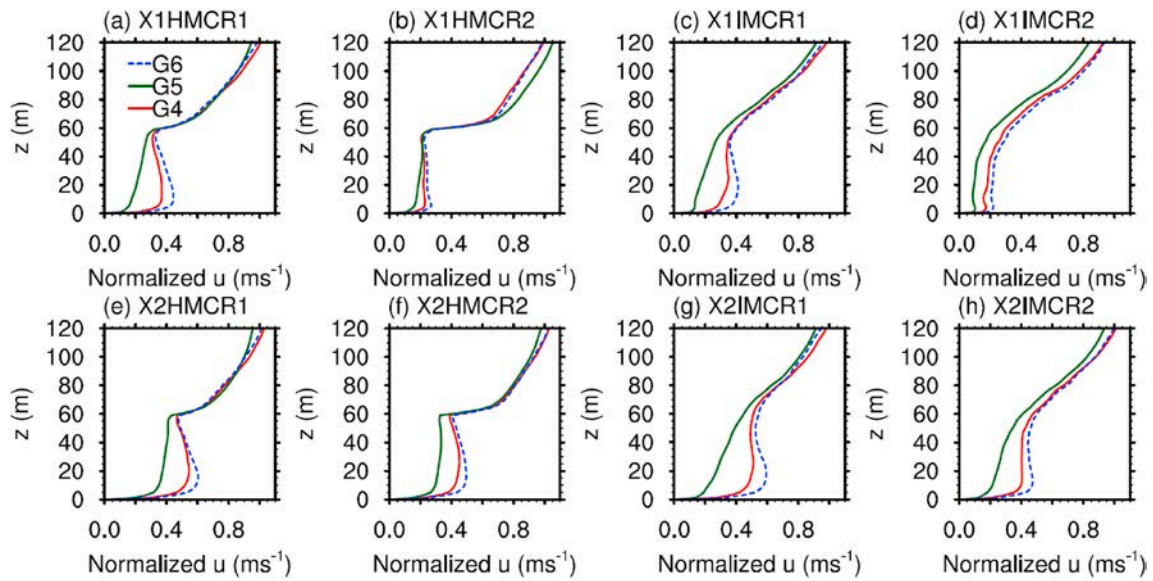


Fig. 9. U-wind profiles in the urban area of thermal scenarios. Only profiles below 120 m are displayed to enlarge the differences between different scenarios. The profile is normalized by its input velocity. Each panel presents one urban form combination, and different line styles (colors) denote different groups (G4, G5, and G6). G4 represents the T1 thermal scenario and 1.5 ms^{-1} input velocity (V1.5), G5 represents the T1 thermal scenario and 3.0 ms^{-1} input velocity (V3.0), and G6 represents the T2 thermal scenario and 1.5 ms^{-1} input velocity (V1.5). (For interpretation of the references to color in this figure legend, the reader is referred to the Web version of this article.)

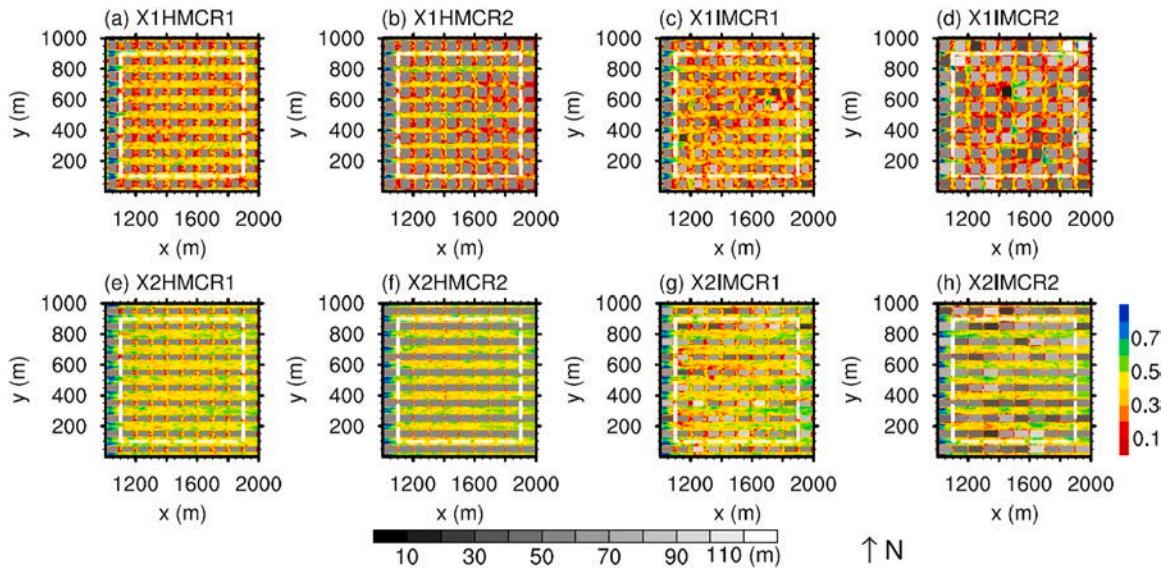


Fig. 10. LES-computed velocity ratios in the urban area of thermal scenarios. Scenarios in G4 (mean building height = 60 m, input wind speed = 1.5 ms^{-1} , T1 thermal condition) are demonstrated. The dashed white box encloses the assessment area with a 100 m wide buffer zone from the lateral boundary.

in greater bottom potential temperature (θ_0 in Eq. (4)). There are very few data regarding Ri_b in urban areas. Nakamura and Oke measured the temperature and wind distribution in a real street canyon and provided an Ri_b range from -0.45 to -0.17 on a clear midsummer afternoon [69], which implies that ground surface heating is reasonable.

4.3. Coupling of mechanical and thermal effects

Fig. 10 shows LES-computed velocity ratios in the urban area of thermal scenarios. It suggests that though the unstable conditions can introduce a strong influence on urban ventilation, the impact of urban form cannot be ignored. Scenarios with better ventilation under neutral conditions will still have better ventilation under the same thermal conditions. For instance, X2 scenarios have obviously better pedestrian-

level ventilation performance compared with X1 scenarios. Consequently, it can be concluded that ventilation performance is affected by both mechanical and thermal conditions. Based on the current experimental settings, the different geometric combinations obtained site-averaged velocity ratios of 0.11–0.25 under neutral conditions, while thermal conditions (T1 and T2) increased these values to 0.28–0.49 (Table 2).

4.3.1. Reaction of ventilation to urban heat

As shown in Fig. 9, heating will affect the vertical distribution of wind speed through intensifying vertical mixing by thermal turbulence, hence enhancing pedestrian-level ventilation. While Fig. 11 shows the LES-computed horizontal distribution of potential temperature in the urban area, and it indicates that better ventilation means greater cooling

Table 3
Bulk Richardson number (Rib) of 40 scenarios under thermal conditions.

Thermal condition		T1		T2		T3		T4	
Mean building height		H60		H60		H60		H60	
Input velocity		V1.5		V3		V1.5		V1.5	
Urban form except mean building height	X1HMCR1	-0.08	-0.03	-0.11	-0.06	-0.43			
	X1HMCR2	-0.11	-0.03	-0.15	-0.08	-0.31			
	X1IMCR1	-0.09	-0.03	-0.12	-0.08	-0.28			
	X1IMCR2	-0.10	-0.03	-0.14	-0.08	-0.33			
	X2HMCR1	-0.04	-0.02	-0.05	-0.03	-0.32			
	X2HMCR2	-0.03	-0.01	-0.03	-0.01	-0.35			
	X2IMCR1	-0.05	-0.02	-0.05	-0.04	-0.32			
	X2IMCR2	-0.05	-0.02	-0.04	-0.03	-0.32			
Group ID		G4	G5	G6	G7	G8			

effects under the same initial thermal conditions. Due to differences in the actual area of walls and roofs in different urban scenarios, the total heat-releasing flux could be slightly different. However, the horizontal distribution of potential temperature under the T2 thermal condition (Fig. 11) demonstrates that at the same vertical level (2 m above the ground), X2 scenarios with a greater velocity ratio do have a lower potential temperature. In contrast, in X1 scenarios with poor ventilation, heat is pushed by the wind and accumulates in the back of the urban scenario; consequently, the worse the ventilation, the higher the temperature in the back of the scenario. In general, the reaction of ventilation to urban heat can be clearly identified in LES experiments. In other words, the LES model captures the fact that ventilation can mitigate urban heat.

4.3.2. Interaction between mechanical and thermal conditions

Under weak background wind, thermal turbulence enhances vertical mixing and thus strengthens near-surface ventilation. However, if the initial thermal conditions are fixed, higher absolute wind speed means stronger horizontal convection, which will weaken the vertical mixing caused by thermal turbulence and eventually lead to the weakening of pedestrian-level ventilation. This is demonstrated by the u-wind profiles of various LES experiments with different input velocity and initial thermal conditions shown in Fig. 9. It is found that u-wind speeds below the mean building height of G5 scenarios (T1 thermal scenario and 3.0 ms^{-1} input wind speed) are much smaller than those of G4 scenarios (T1 thermal scenario and 1.5 ms^{-1} input wind speed), which is consistent with the site-averaged velocity ratio (Table 2).

Furthermore, the potential temperature profiles in Fig. 12 indicate that under the same initial thermal condition (T1), a higher background wind speed leads to a lower air temperature in and above the urban canopy layer (G5 compared with G4). In some cases, the air temperature of G5 may be higher than that of G4, which is due to the lack of ventilation near the ground. However, the potential temperature profiles cannot prove that the vertical movement of airflow is weakened. In order to further confirm that vertical motion is weakened when horizontal convection is strong, Figs. 13 and 14 show the vertical streamlines under different scenarios for cross-building arrays and street canyons, respectively. Taking the X1HMCR1 and X1HMCR2 scenarios as examples, this suggests that in sections either across the street canyon or the building array, the airflow in G4 scenarios has a stronger downward-invading potential.

Similar to Eq. (7), the decreasing rates for the site-averaged velocity ratio between an input wind speed of 3.0 m s^{-1} and 1.5 m s^{-1} under the same T1 thermal condition are calculated as:

$$(VR_{V3.0} - VR_{V1.5}) / VR_{V1.5} \times 100\% \quad (8)$$

Where $VR_{V1.5}$ and $VR_{V3.0}$ are the site-averaged velocity ratios of the G4 and G5 scenarios, respectively. When the input velocity increases from 1.5 m s^{-1} to 3.0 m s^{-1} under the T1 thermal condition, the decreasing rate of the site-averaged velocity ratio ranges from 28.1% (X1HMCR1) to 42.8% (X1HMCR2), with a mean of 36.4% for the eight scenarios.

5. Discussion

The influences of urban form, i.e., its mechanical effects on urban ventilation, have been discussed in the published literature, and how urban thermal conditions affect the airflow in street canyons has been also investigated in previous research. This study demonstrates the coupled effects of both mechanical and thermal conditions on urban ventilation, which has rarely been examined.

In a complex urban environment, there will be many factors both geometric and thermal that can affect airflow, and some important factors may have been ignored, for example scattered building arrays and input wind direction with an angle. Moreover, thermal conditions are simply initialized by a potential temperature profile and sensible heat flux from building walls and roofs. Additionally, because we focused on high-rise and high-density urban scenarios, which represent the current situation of some Asian cities, the mean building height was set to 60 m. Although a set of scenarios with 30 m mean building height

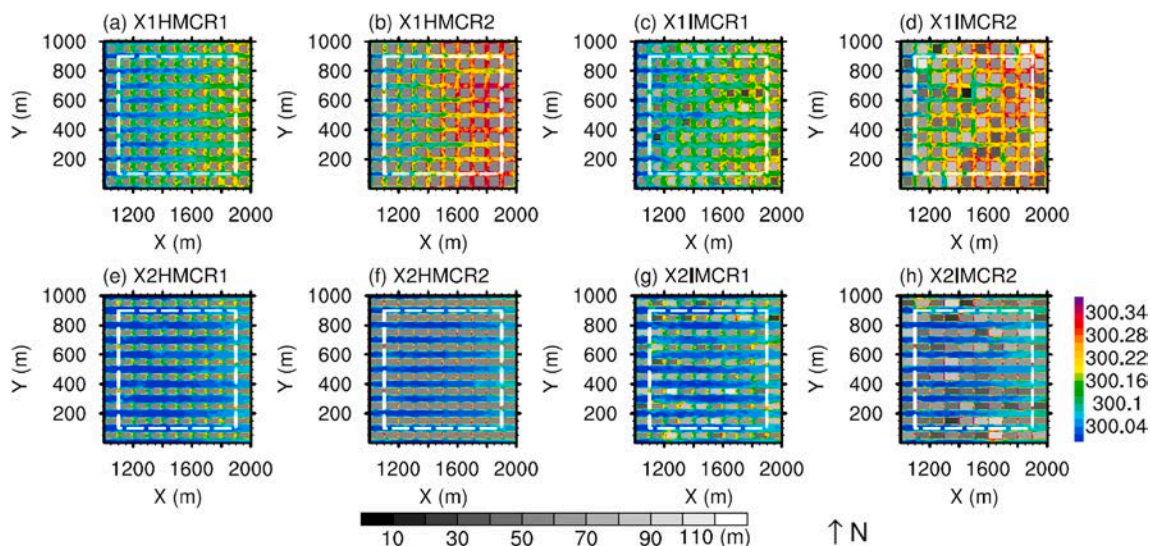


Fig. 11. LES-computed horizontal distribution of potential temperature in the urban area. Scenarios in G6 (mean building height = 60 m, input wind speed = 1.5 ms^{-1} , T2 thermal condition) are demonstrated. The dashed white box encloses the assessment area with a 100 m wide buffer zone from the lateral boundary.

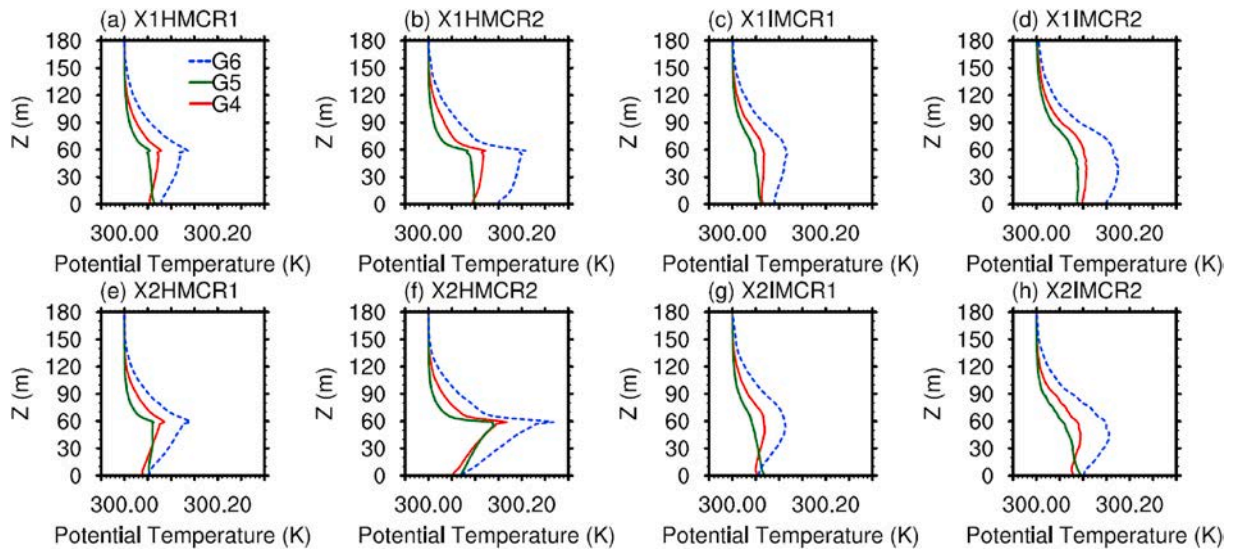


Fig. 12. Potential temperature profiles in the urban area for all thermal scenarios. Only profiles below 120 m are displayed to enlarge the differences between the different scenarios. Each panel presents one geometric combination, and different line styles (colors) denote different groups (G4, G5, and G6). G4 represents the T1 thermal scenario and 1.5 m s^{-1} input velocity (V1.5), G5 represents the T1 thermal scenario and 3.0 m s^{-1} input velocity (V3.0), and G6 represents the T2 thermal scenario and 1.5 m s^{-1} input velocity (V1.5). (For interpretation of the references to color in this figure legend, the reader is referred to the Web version of this article.)

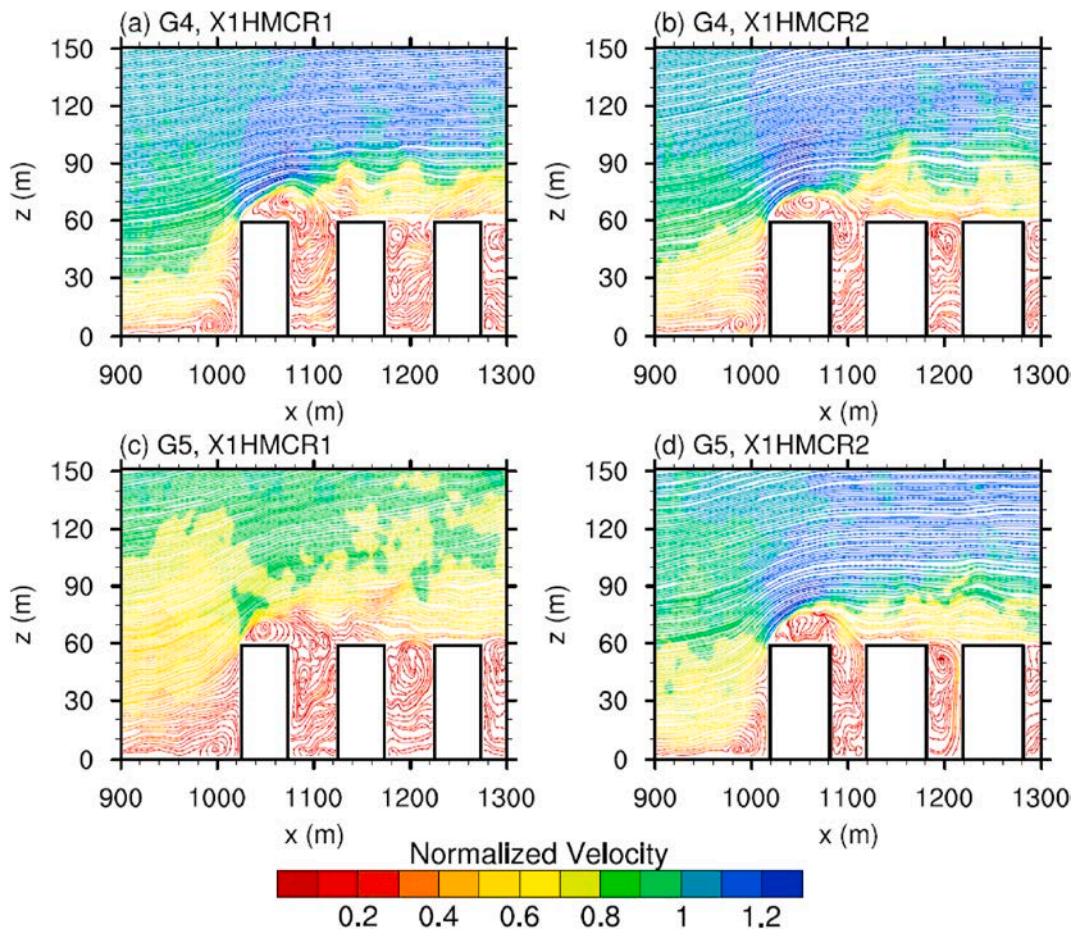


Fig. 13. Vertical streamlines of scenario (a) X1HMCR1 in G4, (b) X1HMCR2 in G4, (c) X1HMCR1 in G5, and (d) X1HMCR2 in G5. Color shading is velocity $(u^2+w^2)^{1/2}$ normalized by the input velocity (1.5 m s^{-1} and 3.0 m s^{-1} for G4 and G5, respectively). The section is taken at $y = 550 \text{ m}$ (cross-building arrays). (For interpretation of the references to color in this figure legend, the reader is referred to the Web version of this article.)

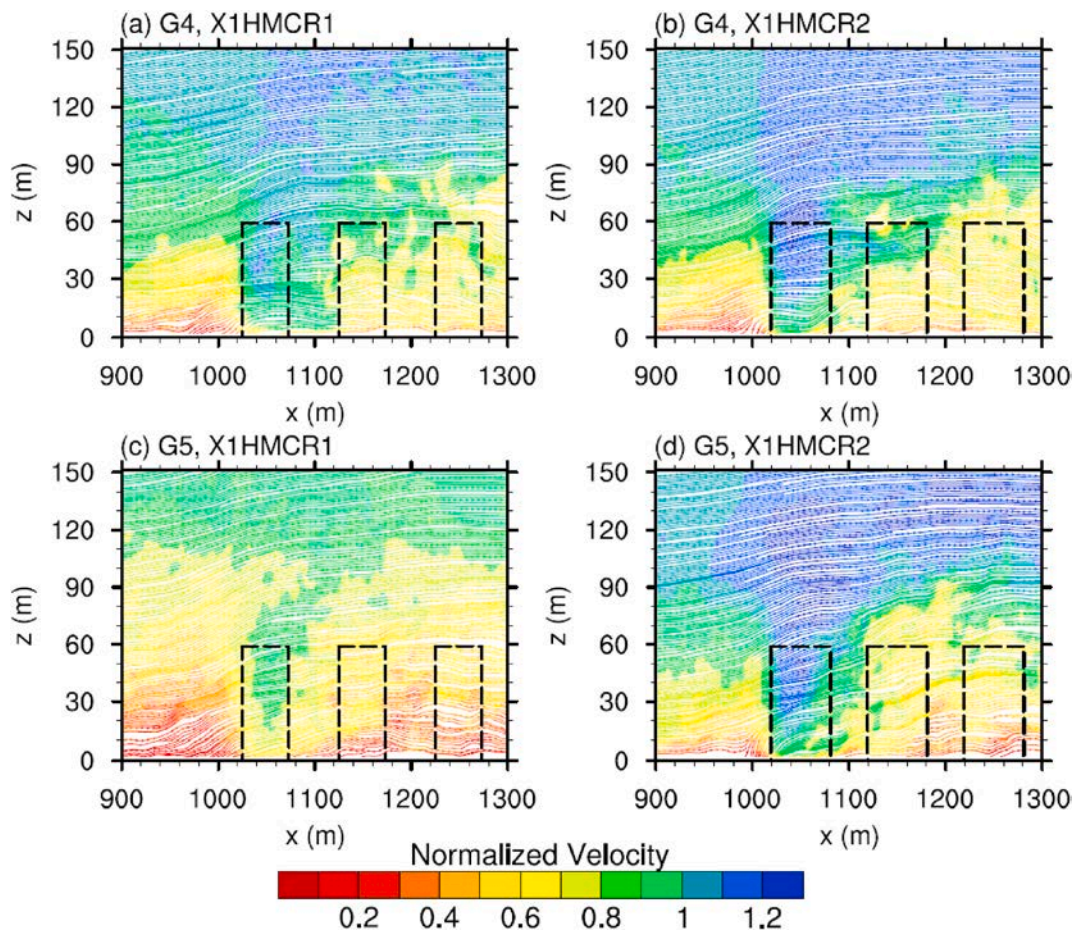


Fig. 14. Vertical streamlines of scenario (a) X1HMCR1 in G4, (b) X1HMCR2 in G4, (c) X1HMCR1 in G5, and (d) X1HMCR2 in G5. Color shading is velocity $(u^2+w^2)^{1/2}$ normalized by the input velocity (1.5 m s^{-1} and 3.0 m s^{-1} for G4 and G5, respectively). The section is taken at $y = 500 \text{ m}$ (cross street canyons). (For interpretation of the references to color in this figure legend, the reader is referred to the Web version of this article.)

were also simulated and the results compared, this building height setting was still higher than heights commonly used in previous studies.

Under neutral conditions, the mechanical effects of urban geometry on the pedestrian-level wind environment have been widely studied. The main contribution of this study is considering the thermal effect. The heat flux implied on building surfaces was only 0.01 and 0.02 Kms^{-1} (about 11.75 and 23.5 Wm^{-2}), which is much smaller than that applied in Gronemeier, Raasch [37] (about 200 Wm^{-2}), but comparable with that of Wang and Li [35] (37 Wm^{-2}). At present, the appropriate range of heat flux that should be adopted in such simulations is unclear. The current study is limited by finite scenario simulations; hence it is still difficult to draw a general conclusion. In addition to heating on rooftops and vertical walls, it is reasonable to prescribe ground surface heating.

6. Conclusions

Based on these scenario designs and simulations, we summarize the main conclusions from the following three aspects: the mechanical effect, the thermal effect, and the coupling effect.

First, under neutral conditions, input velocity has no impact on pedestrian-level ventilation. The H/W ratio is an insufficient indicator of flow regimes for tall building arrays, while absolute building spacing should be considered. Canonical flow regimes can be “horizontally” applied to pedestrian-level ventilation, as the horizontal wake interference between perpendicular and parallel streets slows down the mean wind in the parallel street canyons. Inhomogeneous building heights generate more vertical momentum in street canyons by capturing more downward-propagated momentum fluxes, and they have a negative

(positive) effect on the pedestrian-level velocity of low-roughness (high-roughness) urban fabrics.

Second, under weak background wind, the higher wind speed in the thermal cases is due to the additional convective motion caused by heating from the buildings, which increases vertical mixing throughout the boundary layer in and above the urban area and leads to the higher pedestrian-level velocity ratios compared to the neutral case. Stronger heating results in stronger vertical mixing over the urban blocks, producing higher velocity ratios. Different heating from vertical walls has little effect on pedestrian-level ventilation if the total heat flux is fixed, while ground surface heating improves pedestrian-level ventilation compared with heating from only vertical walls.

Third, better ventilation means greater cooling effects under the same initial thermal conditions. Under weak background wind, thermal turbulence enhances vertical mixing and thus strengthens near-surface ventilation. However, if the initial thermal conditions are fixed, higher absolute wind speed means stronger horizontal convection, which will weaken the vertical mixing caused by thermal turbulence, eventually leading to the weakening of pedestrian-level ventilation.

Declaration of competing interest

The authors declare that they have no known competing financial interests or personal relationships that could have appeared to influence the work reported in this paper.

Acknowledgments

This study was supported by the National Natural Science Foundation of China (Grant No. 41875010), the Special Fund Project for Science and Technology Innovation Strategy of Guangdong Province (Grant No. 2019B121205004), and the Chinese University of Hong Kong (Grant No. 4930785). The authors would like to thank the Planning Department of Hong Kong S.A.R. for the availability of wind tunnel tests and field measurements. Computational resources in the study are supported by the High-Performance Public Computing Service Platform of Jinan University.

References

- P. Coseo, L. Larsen, How factors of land use/land cover, building configuration, and adjacent heat sources and sinks explain urban heat islands in Chicago, *Landscape Urban Plann.* 125 (2014) 117–129.
- Y. Tominaga, T. Stathopoulos, Ten questions concerning modeling of near-field pollutant dispersion in the built environment, *Build. Environ.* 105 (2016) 390–402.
- W. Wang, W. Zhou, E.Y.Y. Ng, Y. Xu, Urban heat islands in Hong Kong: statistical modeling and trend detection, *Nat. Hazards* 83 (2016) 885–907.
- X. Shi, Y. Zhu, J. Duan, R. Shao, J. Wang, Assessment of pedestrian wind environment in urban planning design, *Landscape Urban Plann.* 140 (2015) 17–28.
- L. Chen, J. Hang, M. Sandberg, L. Claesson, S. Di Sabatino, H. Wigo, The impacts of building height variations and building packing densities on flow adjustment and city breathability in idealized urban models, *Build. Environ.* 118 (2017) 344–361.
- J. Hang, Y. Li, M. Sandberg, R. Buccolieri, S. Di Sabatino, The influence of building height variability on pollutant dispersion and pedestrian ventilation in idealized high-rise urban areas, *Build. Environ.* 56 (2012) 346–360.
- R. Buccolieri, P. Salizzoni, L. Souhac, V. Garbero, S. Di Sabatino, The breathability of compact cities, *Urban Clim.* 13 (2015) 73–93.
- R. Buccolieri, J. Hang, Recent advances in urban ventilation assessment and flow modelling, *Atmosphere* 10 (2019).
- R.E. Britter, S.R. Hanna, Flow and dispersion in urban areas, *Annu. Rev. Fluid Mech.* 35 (2003) 469–496.
- E. Ng, C. Yuan, L. Chen, C. Ren, J.C.H. Fung, Improving the wind environment in high-density cities by understanding urban morphology and surface roughness: a study in Hong Kong, *Landscape Urban Plann.* 101 (2011) 59–74.
- B. Blocken, T. Stathopoulos, J.P.A.J. van Beeck, Pedestrian-level wind conditions around buildings: review of wind-tunnel and CFD techniques and their accuracy for wind comfort assessment, *Build. Environ.* 100 (2016) 50–81.
- M. Skote, M. Sandberg, U. Westerberg, L. Claesson, A. Johansson, Numerical and experimental studies of wind environment in an urban morphology, *Atmos. Environ.* 39 (2005) 6147–6158.
- T.R. Oke, G. Mills, A. Christen, J.A. Voogt, *Urban Climates*, Cambridge University Press, 2017.
- S.-J. Mei, J.-T. Hu, D. Liu, F.-Y. Zhao, Y. Li, Y. Wang, et al., Wind driven natural ventilation in the idealized building block arrays with multiple urban morphologies and unique package building density, *Energy Build.* 155 (2017) 324–338.
- Y.-K. Ho, C.-H. Liu, M.S. Wong, Preliminary study of the parameterisation of street-level ventilation in idealised two-dimensional simulations, *Build. Environ.* 89 (2015) 345–355.
- M. Lin, J. Hang, Y. Li, Z. Luo, M. Sandberg, Quantitative ventilation assessments of idealized urban canopy layers with various urban layouts and the same building packing density, *Build. Environ.* 79 (2014) 152–167.
- Q.M. Zahid Iqbal, A.L.S. Chan, Pedestrian level wind environment assessment around group of high-rise cross-shaped buildings: effect of building shape, separation and orientation, *Build. Environ.* 101 (2016) 45–63.
- J. Hang, Z. Luo, M. Sandberg, J. Gong, Natural ventilation assessment in typical open and semi-open urban environments under various wind directions, *Build. Environ.* 70 (2013) 318–333.
- C. Yuan, E. Ng, Building porosity for better urban ventilation in high-density cities – a computational parametric study, *Build. Environ.* 50 (2012) 176–189.
- C.-Y. Wen, Y.-H. Juan, A.-S. Yang, Enhancement of city breathability with half open spaces in ideal urban street canyons, *Build. Environ.* 112 (2017) 322–336.
- Y.-H. Juan, A.-S. Yang, C.-Y. Wen, Y.-T. Lee, P.-C. Wang, Optimization procedures for enhancement of city breathability using arcade design in a realistic high-rise urban area, *Build. Environ.* 121 (2017) 247–261.
- K.T. Tse, X. Zhang, A.U. Weerasuriya, S.W. Li, K.C.S. Kwok, C.M. Mak, et al., Adopting ‘lift-up’ building design to improve the surrounding pedestrian-level wind environment, *Build. Environ.* 117 (2017) 154–165.
- X. Zhang, K.T. Tse, A.U. Weerasuriya, S.W. Li, K.C.S. Kwok, C.M. Mak, et al., Evaluation of pedestrian wind comfort near ‘lift-up’ buildings with different aspect ratios and central core modifications, *Build. Environ.* 124 (2017) 245–257.
- X. Zhang, K.T. Tse, A.U. Weerasuriya, K.C.S. Kwok, J. Niu, Z. Lin, et al., Pedestrian-level wind conditions in the space underneath lift-up buildings, *J. Wind Eng. Ind. Aerod.* 179 (2018) 58–69.
- R. Ramponi, B. Blocken, L.B. de Co, W.D. Janssen, CFD simulation of outdoor ventilation of generic urban configurations with different urban densities and equal and unequal street widths, *Build. Environ.* 92 (2015) 152–166.
- Y. He, A. Tablada, N.H. Wong, A parametric study of angular road patterns on pedestrian ventilation in high-density urban areas, *Build. Environ.* 151 (2019) 251–267.
- Z.T. Ai, C.M. Mak, CFD simulation of flow in a long street canyon under a perpendicular wind direction: evaluation of three computational settings, *Build. Environ.* 114 (2017) 293–306.
- Y. Dai, C.M. Mak, Z. Ai, J. Hang, Evaluation of computational and physical parameters influencing CFD simulations of pollutant dispersion in building arrays, *Build. Environ.* 137 (2018) 90–107.
- S. Liu, W. Pan, H. Zhang, X. Cheng, Z. Long, Q. Chen, CFD simulations of wind distribution in an urban community with a full-scale geometrical model, *Build. Environ.* 117 (2017) 11–23.
- J.F. Barlow, Progress in observing and modelling the urban boundary layer, *Urban Clim.* 10 (2014) 216–240.
- S.-J. Mei, J.-T. Hu, D. Liu, F.-Y. Zhao, Y. Li, H.-Q. Wang, Thermal buoyancy driven canyon airflows inside the compact urban blocks saturated with very weak synoptic wind: plume merging mechanism, *Build. Environ.* 131 (2018) 32–43.
- N. Nazarian, J. Kleissl, Realistic solar heating in urban areas: air exchange and street-canyon ventilation, *Build. Environ.* 95 (2016) 75–93.
- S.-B. Park, J.-J. Baik, A large-eddy simulation study of thermal effects on turbulence coherent structures in and above a building array, *J. Appl. Meteorol. Climatol.* 52 (2013) 1348–1365.
- S.J. Mei, C.W. Liu, D. Liu, F.Y. Zhao, H.Q. Wang, X.H. Li, Fluid mechanical dispersion of airborne pollutants inside urban street canyons subjected to multi-component ventilation and unstable thermal stratifications, *Sci. Total Environ.* 565 (2016) 1102–1115.
- X. Wang, Y. Li, Predicting urban heat island circulation using CFD, *Build. Environ.* 99 (2016) 82–97.
- L. Yang, Y. Li, Thermal conditions and ventilation in an ideal city model of Hong Kong, *Energy Build.* 43 (2011) 1139–1148.
- T. Gronemeier, S. Raasch, E. Ng, Effects of unstable stratification on ventilation in Hong Kong, *Atmosphere* 8 (2017).
- W. Wang, E. Ng, Air ventilation assessment under unstable atmospheric stratification — a comparative study for Hong Kong, *Build. Environ.* 130 (2018) 1–13.
- B. Maronga, M. Gryscha, R. Heinze, F. Hoffmann, F. Kanani-Sühring, M. Keck, et al., The Parallelized Large-Eddy Simulation Model (PALM) version 4.0 for atmospheric and oceanic flows: model formulation, recent developments, and future perspectives, *Geosci. Model Dev. (GMD)* 8 (2015) 2515–2551.
- U. Schumann, Subgrid scale model for finite difference simulations of turbulent flows in plane channels and annuli, *J. Comput. Phys.* 18 (1975) 376–404.
- C.H. Moeng, J.C. Wyngaard, Spectral analysis of large-eddy simulations of the convective boundary layer, *J. Atmos. Sci.* 45 (1988) 3573–3587.
- E.M. Saiki, C.H. Moeng, P.P. Sullivan, Large-eddy simulation of the stably stratified planetary boundary layer, *Boundary-Layer Meteorol.* 95 (2000) 1–30.
- J.W. Deardorff, Stratocumulus-capped mixed layers derived from a three-dimensional model, *Boundary-Layer Meteorol.* 18 (1980) 495–527.
- C. Temperton, A generalized prime factor FFT algorithm for any $N = 2^p 3^q 5^r$, *SIAM J. Sci. Stat. Comput.* (1992) 676–686.
- J.H. Williamson, Low-storage Runge-Kutta schemes, *J. Comput. Phys.* 35 (1980) 48–56.
- S.A. Piacsek, G.P. Williams, Conservation properties of convection difference schemes, *J. Comput. Phys.* 198 (1970) 580–616.
- L.J. Wicker, W.C. Skamarock, Time-splitting methods for elastic models using forward time schemes, *Mon. Weather Rev.* 130 (2002) 2088–2097.
- M. Briscolini, P. Santangelo, Development of the mask method for incompressible unsteady flows, *J. Comput. Phys.* 84 (1989) 57–75.
- J. Hang, M. Sandberg, Y. Li, Age of air and air exchange efficiency in idealized city models, *Build. Environ.* 44 (2009) 1714–1723.
- M. Kurppa, A. Hellsten, M. Auvinen, S. Raasch, T. Vesala, L. Jarvi, Ventilation and air quality in city blocks using large-eddy simulation-urban planning perspective, *Atmosphere* 9 (2018) 1–27.
- E. Ng, Policies and technical guidelines for urban planning of high-density cities – air ventilation assessment (AVA) of Hong Kong, *Build. Environ.* 44 (2009) 1478–1488.
- W. Wang, T. Yang, Y. Li, Y. Xu, M. Chang, X. Wang, Identification of pedestrian-level ventilation corridors in downtown Beijing using large-eddy simulations, *Build. Environ.* 182 (2020), 107169.
- M.O. Letzel, M. Krane, S. Raasch, High resolution urban large-eddy simulation studies from street canyon to neighbourhood scale, *Atmos. Environ.* 42 (2008) 8770–8784.
- T.S. Lund, X. Wu, K.D. Squires, Generation of turbulent inflow data for spatially-developing boundary layer simulations, *J. Comput. Phys.* 140 (1998) 233–258.
- H. Kataoka, M. Mizuno, Numerical flow computation around aeroelastic 3D square cylinder using inflow turbulence, *Wind Struct.* 5 (2002) 379–392.
- B. Maronga, M. Gryscha, R. Heinze, F. Hoffmann, F. Kanani-Sühring, M. Keck, et al., The Parallelized Large-Eddy Simulation Model (PALM) version 4.0 for atmospheric and oceanic flows: model formulation, recent developments, and future perspectives, *Geosci. Model Dev. Discuss. (GMDD)* 8 (2015) 1539–1637.
- M. Keck, S. Raasch, M.O. Letzel, E. Ng, First results of high resolution large-eddy simulations of the atmospheric boundary layer, *J. Heat Island Instit. Int.* 9 (2014) 39–43.
- M.O. Letzel, C. Helmke, E. Ng, X. An, A. Lai, S. Raasch, LES case study on pedestrian level ventilation in two neighbourhoods in Hong Kong, *Meteorol. Z.* 21 (2012) 575–589.

- [59] M. Kanda, A. Inagaki, T. Miyamoto, M. Gryschka, S. Raasch, A new aerodynamic parameterization for real urban surfaces, *Boundary-Layer Meteorol.* 148 (2013) 357–377.
- [60] A.A. Razak, A. Hagishima, N. Ikegaya, J. Tanimoto, Analysis of airflow over building arrays for assessment of urban wind environment, *Build. Environ.* 59 (2013) 56–65.
- [61] A. Inagaki, M.C.L. Castillo, Y. Yamashita, M. Kanda, H. Takimoto, Large-eddy simulation of coherent flow structures within a cubical canopy, *Boundary-Layer Meteorol.* 142 (2011) 207–222.
- [62] S.-B. Park, J.-J. Baik, Large-eddy simulations of convective boundary layers over flat and urbanlike surfaces, *J. Atmos. Sci.* 71 (2014) 1880–1892.
- [63] Y. Tominaga, A. Mochida, R. Yoshie, H. Kataoka, T. Nozu, M. Yoshikawa, et al., AIJ guidelines for practical applications of CFD to pedestrian wind environment around buildings, *J. Wind Eng. Ind. Aerod.* 96 (2008) 1749–1761.
- [64] W. Wang, E. Ng, C. Yuan, S. Raasch, Large-eddy simulations of ventilation for thermal comfort — a parametric study of generic urban configurations with perpendicular approaching winds, *Urban Clim.* 20 (2017) 202–227.
- [65] W. Wang, Y. Xu, E. Ng, Large-eddy Simulations of Pedestrian-Level Ventilation for Assessing a Satellite-Based Approach to Urban Geometry Generation, *Graphical Models*, 2017.
- [66] K. Uehara, S. Murakami, S. Oikawa, S. Wakamatsu, Wind tunnel experiments on how thermal stratification affects flow in and above urban street canyons, *Atmos. Environ.* 34 (2000) 1553–1562.
- [67] S.-B. Park, J.-J. Baik, S. Raasch, M.O. Letzel, A large-eddy simulation study of thermal effects on turbulent flow and dispersion in and above a street canyon, *J. Appl. Meteorol. Climatol.* 51 (2012) 829–841.
- [68] N. Ikegaya, A. Hagishima, J. Tanimoto, Y. Tanaka, K-i Narita, S.A. Zaki, Geometric dependence of the scalar transfer efficiency over rough surfaces, *Boundary-Layer Meteorol.* 143 (2012) 357–377.
- [69] Y. Nakamura, T.R. Oke, Wind, temperature and stability condition in an East-West oriented urban canyon, *Atmos. Environ.* 22 (1988) 2691–2700.